Heliyon 10 (2024) e39389

Contents lists available at ScienceDirect

Heliyon

journal homepage: www.cell.com/heliyon

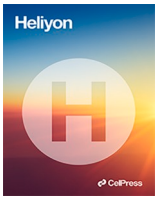

Research article

Investigating intermittent immersion during osmotic dehydration of mango (*Mangifera indica* L. Moench). Part B mathematical modeling of D2I and D3I kinetics in mango (*Mangifera indica* L. Moench) slices

C. Tsopwo Zena [a], Y. Jiokap Nono [b,*]

[a] *Department of Process Engineering, National Advanced School of Agro-industrial Sciences, ENSAI, Ngaoundere University, P.O. Box 455, Ngaoundere, Cameroon*
[b] *Department of Chemical Engineering and Environment, UIT, Ngaoundere University, P.O. Box 455, Ngaoundere, Cameroon*

A R T I C L E I N F O

Keywords:
Mango
Dehydration impregnation by immersion
Intermittence
Modeling
Modified Crank II model
Activation energy

A B S T R A C T

This work aims to investigate the dynamics of water loss (WL) and solute gain (SG) during dehydration impregnation by immersion (D2I) and intermittent immersion (D3I). WL and SG of mango slices, 4 × 1× 1 cm^3 in size, during dehydration immersion impregnation (D2I) and dehydration impregnation by intermittent immersion (D3I) were determined at 35, 45 and 55 °C for 270 min. Mango slices were immersed in a hypertonic sucrose solution of (61.6 ± 0.2) °Brix at a ratio of 6 mL of hypertonic solution per gram of fruit. Five semi-empirical models, two of which have been modified, were used to study mass transfer during D2I and D3I, namely the Azura, Weibull, Crank, Modified Crank I, and Modified Crank II models. The equilibrium water loss (WL_∞), the equilibrium solute gain (SG_∞), the diffusion coefficient, and activation energy were determined using the Modified Crank II model which was the best of all the tested models. Equilibrium water loss during D2I decreased with increasing temperature, while during D3I it increased with temperature. The SG_∞ during D2I and D3I increases with temperature but was higher in D2I than in D3I. The average water diffusion coefficients were (6.02 ± 2.62) × 10^{-8} m^2 s^{-1} for D2I and (4.89 ± 0.55) × 10^{-8} m^2 s^{-1} for D3I and the average solute diffusion coefficients were (4.45 ± 0.53) × 10^{-8} m^2 s^{-1} for D2I and (8.33 ± 0.79) × 10^{-8} m^2 s^{-1} for D3I. The activation energies for WL in D2I and D3I were respectively 38789 J mol^{-1} and 9503 J mol^{-1}. The respective values for SG were 9037 J mol^{-1} and 7327 J mol^{-1}. This work demonstrates that mass transfers in D3I are better than those in D2I, and it highlights that, unlike the D2I process, the D3I process is less sensitive to temperature variations, making it particularly advantageous for processing products with high nutritional value.

Nomenclature

C_z	Shape correction factor (dimensionless)
D	Diffusion coefficient ($m^2 \cdot s^{-1}$)
D_0	Arrhenius factor, generally defined as the reference diffusion coefficient at an infinitely high temperature ($m^2 \cdot s^{-1}$)

(*continued on next page*)

* Corresponding author.
E-mail address: jiokapnonoy@yahoo.fr (Y. Jiokap Nono).

https://doi.org/10.1016/j.heliyon.2024.e39389
Received 21 February 2024; Received in revised form 11 October 2024; Accepted 14 October 2024
Available online 15 October 2024

(*continued*)

D_e	Effective diffusivity ($m^2 \cdot s^{-1}$)
E_a	The activation energy of diffusion ($J \cdot mol^{-1}$)
k	Diffusion kinetics constant (min^{-1})
L_C	Half the thickness of the slab or characteristic length (m)
M	Sample mass (g)
MRE	Mean relative error (dimensionless)
n	Number of observations (dimensionless)
p	Number of model parameters (dimensionless)
R	Universal gas constant ($J \cdot mol^{-1} \cdot K^{-1}$)
RMSE	Root mean square error (dimensionless)
R^2	Coefficient of determination (dimensionless)
R^2_{adj}	Adjusted coefficient of determination (dimensionless)
s	Parameters that can be defined as relative rate constant (min)
SG	Solute gain (g/100 g w-b)
SG_∞	Solid gain at equilibrium condition (g/100 g w-b)
t	Time (min)
T	Temperature (K)
WL	Water loss (g/100 g w-b)
WL_∞	Water loss at equilibrium condition (g/100 g w-b)
x	Spatial coordinate in one-dimensional transfer (m)
X_{wo}	Weight fraction of water (g/g w-b)
$y_{i,calc}$:	Predicted WL or SG
$y_{i,exp}$	Experimental WL or SG
Y	The concentration of the diffusing material (g/100 g w-b)
Σmin	Minimum sum ranking criterion (dimensionless)
α	Scale parameter of the Weibull's model (min)
β	Shape parameter (dimensionless)
Subscripts	
w	Water
s	Solute
0	Initial
t	Time

1. Introduction

Dehydration of fruits and vegetables by immersion in hypertonic solutions, known as osmotic dehydration (OD) also called dehydration impregnation by immersion (D2I), has been the subject of several studies in recent decades. There are several advantages of D2I. It is a low-temperature water removal process, that minimizes color and flavor loss, improves texture and product stability, and enhances nutrient retention during storage. It is easy to implement, requires basic equipment, and has been reported to reduce energy consumption, speed up post-drying time, and preserve the structure of food products [1]. The other advantage of D2I is associated with the absorption of solutes by the food, leading to an improvement in the taste and sensory attributes of the final products [2]. One notable benefit of D2I is the prevention of oxidation, thanks to the oxygen-free environment used during the immersion of products in the osmotic solution [3]. This effectively prevents enzymatic and oxidative discoloration, eliminating the need for chemicals, such as Sulphur dioxide, or a blanching process to preserve food quality. By operating at temperatures less than 50 °C, D2I effectively avoids heat-induced damage and prevents browning reactions from occurring [4].

This operation, generally considered as pre-treatment, is a partial dehydration method that consists of immersing a material to be dehydrated in a hypertonic solution of carbohydrates, salt and/or several other solutes. During the D2I process, the liquid (water + soluble substances) present in the biological material diffuses into the hypertonic solution and simultaneously the solutes present in the hypertonic solution migrate from the solution to the biological material [5]. In general, osmotic dehydration is intrinsically slow, and several scientific studies have identified factors that increase the rate of mass transfer without adversely affecting quality. These factors include the intrinsic properties of the biological material (porous structure, size, shape, and surface area of the product) and the D2I operating conditions (time, processing temperature, pressure, solution agitation, and solution composition) [6,7].

To further improve mass transfer, thermal and non-thermal treatments have been developed and it has been shown that these techniques do improve mass transfer during D2I [8]. To join this scientific challenge a new technique based on intermittent immersion has been developed by Tsopwo Zena and Jiokap Nono [8]. This technique is called dehydration impregnation by intermittent immersion (D3I). The intermittent immersion method consists of repeatedly immersing and de-immersing the biological material in a hypertonic solution for a specific process time. The duration of these actions will depend on the nature of the plant material and the specifications. This immersion method has the advantage over the continuous immersion method in that it minimizes solute gain.

Several models have been established to describe the kinetics of mass transfer during osmotic dehydration to understand the effects of variables during the process. The models can be classified as empirical and semi-empirical, phenomenological and mechanistic. Empirical and semi-empirical models offer the advantage of being applicable to non-classical geometries without requiring consideration of the underlying phenomenological mechanisms in the process [9]. Some of them allow the prediction of equilibrium values. Azuara, Peleg, Page, Penetration, and Weibull are examples of this type of model. Phenomenological models can determine the diffusion coefficient, but require equilibrium values and must be used for classical geometries [9]. Crank [10] is the most widely used

phenomenological model, which includes a group of analytical solutions based on Fick's second law [10]. Mechanistic models describe the osmotic dehydration process by considering the cellular structure of the food sample. Assis et al. [11] established equivalences between the parameters of several models for D2I.

All these kinetic studies and modeling were carried out mainly under continuous immersion. At present, no information is available on the dynamics of mass transfer during intermittent immersion. Taking intermittence into account in this process, as presented by Tsopwo Zena and Jiokap Nono [8], would provide additional information for understanding the transfer mechanisms.

This study will involve (i) determining the mass transfer kinetics of water (and sugar) as a function of temperature, (ii) developing and validating a mathematical model for those mass transfer kinetics, and (iii) determining the equilibrium water loss and solute gain, the water (and sugar) diffusion coefficients and the activation energies associated with the D2I and D3I processes as applied to mango slices.

2. Materials and methods

2.1. Preparation of raw materials

The mango (*Mangifera indica* L. Moench) used in this study is locally known as the "coffee mango" variety. This variety is the most widely produced, marketed, and consumed in the Vina department of the Adamawa region of Cameroon [12]. The mangoes, which were at the same maturity level (Brix degree between 12 and 13 %) and showed no signs of deterioration, were purchased from the local market (Dang) in Ngaoundere III and transported to the laboratory for storage before the experiments. The Brix level of the fruits was measured using an ATAGO (Japan) refractometer, with a reading range of 0–32 %. Before each experiment, $4 \times 1 \times 1$ cm^3 mango parallelepiped shape was manually created using a knife and a caliper. The steps are described in Fig. 1.

2.2. Preparation of the hypertonic solution

The hypertonic solutions were prepared using an appropriate quantity of sucrose (food grade, purchased at the local market in Ngaoundere III) and distilled water in proportion to the desired hypertonic solution concentration. Sucrose was chosen as the sole solute due to its lower cost, accessibility, dehydrating power, and organoleptic properties [13,14]. Hypertonic solutions were prepared according to the steps described in Fig. 2. The sucrose concentrations of the hypertonic solutions were assessed at room temperature using a HANNA HI 96801 digital refractometer, which has a reading range of 0–85 %.

2.3. Experimental studies

The D2I and D3I operations were carried out according to the process and procedure described in Fig. 3. They were conducted at 35 °C with a fruit mass/volume hypertonic solution ratio of 1/6 (g/mL) in a hypertonic sucrose solution with a concentration of 61.6 ± 0.2 °Brix. Immersion during D2I was continuous until the end of the process with a process time of 270 min, whereas, immersion during D3I was discontinuous until the end of the process with an immersion time of 21 min, a de-immersion time of 9 min and a process time of 270 min corresponding to 9 intermittent cycles. For D2I, stirring was done manually (six revolutions over 3 s) every 10 min to enhance mass transfer and prevent the formation of a dilute solution film around the samples, whereas for D3I, immersion, and de-immersion were sufficient to prevent the formation of a film of dilute solution around the samples.

After each experiment, the mango slices were removed from the hypertonic medium, drained, rinsed with very little water, drained a second time, and weighed. The water content of the mango slices, treated with D2I or D3I, was then determined to calculate the water loss (WL) and solute gain (SG) in equations (1) and (2) respectively.

$$WL = \frac{M_0 \cdot X_{w0} - M_t \cdot X_{wt}}{M_0} \tag{1}$$

$$SG = WL - \frac{M_0 - M_t}{M_0} \tag{2}$$

with M_0: sample mass, (g), at time t = 0; M_t: sample mass, (g), at time t; X_{wo}: weight fraction of water, (g/g w-b) at time t = 0; X_{wt}: weight fraction of water, (g/g w-b), at time t.

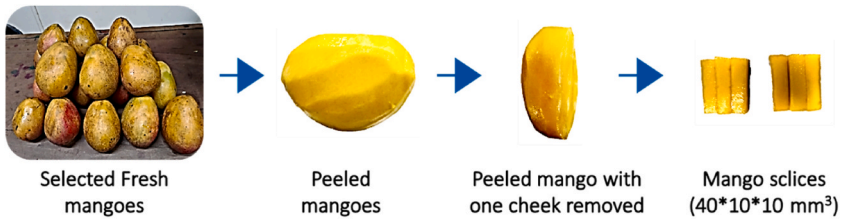

Fig. 1. Steps to obtain the mango slices.

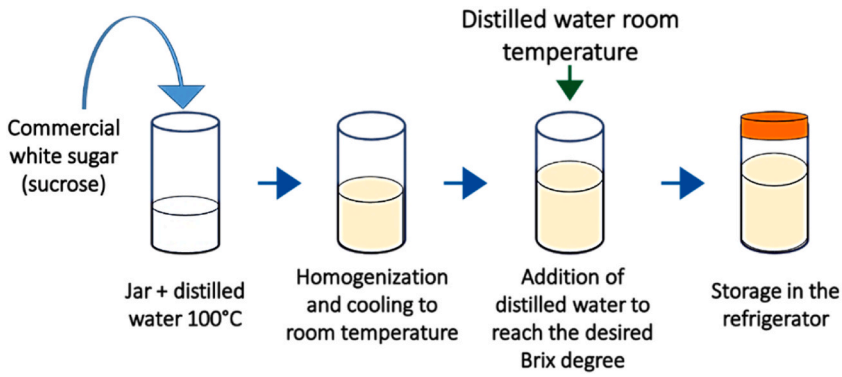

Fig. 2. Step in the production of hypertonic sucrose solution.

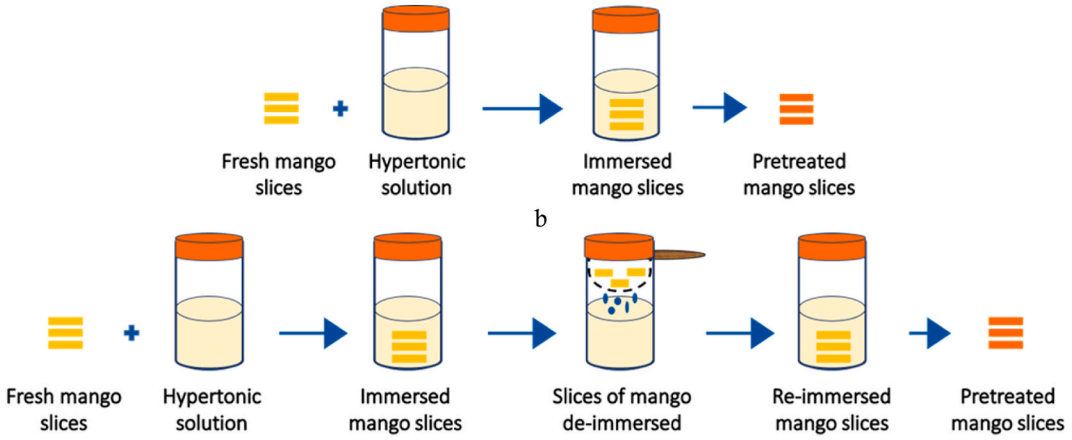

Fig. 3. Operating steps for obtaining mango slices pre-treated with (a) D2I and (b) D3I.

Mass transfer monitoring during D2I and D3I was evaluated by following the evolution of WL and SG as a function of time (0–270 min) and temperature (35, 45, and 55 °C). In the case of D2I, water loss (WL) and solute gain (SG) were evaluated every 30 min, whereas in the case of D3I, WL and SG were evaluated after 21 min of immersion and 9 min of de-immersion, until the end of the process [8]. All tests were repeated three times.

2.4. Modeling of mass transfer kinetics

The mathematical models used to fit the experimental data are the Crank, Azuara, and Weibull models. These models were selected because they are the most effective in the literature for predicting equilibrium mass transfer values and the diffusion coefficient.

2.4.1. Crank's model (1975)

This model is widely used for modeling and analyzing the kinetics of moisture diffusion, particularly in the context of drying [15–20], it has also been used in osmotic dehydration [21–23], to gain insights into how diffusing substances behave under different conditions. Crank [10] provides, for a given condition, analytical solutions to diffusion problems, making it easier to predict how diffusion progresses over time and space. The diffusion equation, for which Crank provides a solution, is Fick's second law, a partial differential equation that represents how the concentration of a substance changes over time and space due to diffusion. The general form of the diffusion equation is presented in equation (3):

$$\frac{\partial Y}{\partial t} = D \cdot \nabla^2 Y \tag{3}$$

where: Y is the concentration of the diffusing material, t is time, and D is the diffusion coefficient.

Analytical solutions of the diffusion equation in Cartesian, cylindrical, or spherical coordinate systems require specific initial and boundary conditions. In most cases, whether dealing with drying or osmotic dehydration, the system under study is typically a finite medium, which results in boundaries at both ends of the domain. In this study, the mango slices are initially $4 \times 1 \times 1$ cm^3 in size, corresponding to the Cartesian coordinate system. Due to the presence of boundary effects, determining how diffusion occurs within a

bounded region with specific initial and boundary conditions is more complex than diffusion in a semi-infinite or infinite medium. This is why simplifying assumptions are adopted. First, it is assumed that diffusion is mainly one-dimensional and that the system is bounded by two parallel planes, making the system a plane sheet of material with thickness L. This thickness is so small that effectively all the diffusing substance enters through the plane faces, with negligible diffusion through the edges (infinite plane geometry) [10]. This is referred to as thin-layer drying, where the thickness of the material layer is considered small relative to its surface area. In this process, the transfer occurs uniformly across the material, predominantly from the exposed surface, with minimal influence from the boundaries. The symmetry of the system allows the study of the diffusion in only half the thickness. Another assumption is that the initial moisture content is uniformly distributed throughout the product, the solution concentration is constant, the shrinkage is negligible, the diffusion coefficient (D) is constant during dehydration and the mass transfer resistance at the product surface is negligible. All these assumptions allow for a simplified analytical solution, which avoids the complexities introduced by the boundaries and makes it easier to model the drying process mathematically. The unidimensional diffusion equation and the concentration Y(x,t) of the diffusing material are respectively given by equations (4) and (5) [24]:

$$\frac{\partial Y(x,t)}{\partial t} = D \bullet \frac{\partial^2 Y(x,t)}{\partial x^2} \tag{4}$$

$$\frac{Y(x,t)}{Y_\infty} = 1 - \boldsymbol{erf}\left(\frac{x}{2 \bullet \sqrt{D \bullet t}}\right) \tag{5}$$

Where **erf** is the error function presented in equation (6):

$$\boldsymbol{erf}(z) = \frac{2}{\sqrt{\pi}} \bullet \int_0^z e^{-u^2} \bullet du \tag{6}$$

Y(x,t) is the concentration of the diffusing material at position x and time t; Y_∞ the equilibrium concentration of the diffusing material; D is the diffusion coefficient of the diffusing material in the system (solid); x is the position in the solid; t is the time; and **erf** is the error function. It can be approximated using various methods, one of which is the series expansion. However, in many practical applications, the error function is computed numerically [10].

When assuming a uniform initial moisture content and infinite solid in a one-dimensional process, and when focusing on the overall process kinetics rather than the concentration distribution within the material, Crank [10] gives an analytical solution that describes the average concentration as a function of time, which is particularly useful and presented in equation (7):

$$\frac{Y}{Y_\infty} = 1 - \frac{8}{\pi^2} \cdot \sum_{n=0}^{\infty} \frac{1}{(2n+1)^2} \exp\left(-(2n+1)^2 \cdot \frac{\pi^2 \cdot D_e}{4 \cdot L_C^2} \cdot t\right) \tag{7}$$

Y: WL or SG is the water loss or solute gain at instant t; Y_∞: WL_∞ or SG_∞ are the water loss or the solid gain at equilibrium condition and L_C: half the thickness of the slab or characteristic length.

Equation (7) is not only used to predict how the average concentration varies over time during the process, but it is also beneficial for fitting experimental process data to estimate the effective diffusivity D_e. The solution is presented as an infinite series, where the terms rapidly converge, making it practical for calculation. In general, equation (7) is applied in two phases: either for the initial moments of the kinetics or for cases involving long drying times (large values of t). For this last case (long drying times), the series can be approximated by just the first term of the series (for n = 0) (equation (8)), because the higher-order terms contribute very little to the overall diffusing material concentration:

$$\frac{Y}{Y_\infty} \approx 1 - \frac{8}{\pi^2} \cdot \exp\left(-\frac{\pi^2 \cdot D_e}{4 \cdot L_C^2} \cdot t\right) \tag{8}$$

This simplified Crank's solution, widely used by authors [16,21] to model the diffusion kinetics and determine the process rate and effective diffusivity, provides a direct relationship between the concentration and process time. These physical quantities are essential parameters for designing and optimizing processes. However, Perry and Green [25] noted that it should be clear that estimates based on relationships assuming constant diffusivity are only approximations. This is because liquid diffusivity in solids typically decreases with moisture concentration, and both liquid and vapor diffusivities change, while the material also shrinks during drying.

At the initial time of the kinetics, the simplified equation (8) is no longer valid, and the complete equation (7) must be used. In early times, employing the full series solution is necessary to accurately capture the initial condition [25]. Indeed, at the initial moment, the ratio $\frac{Y}{Y_\infty}$ is known to be zero. This consideration is not addressed by equation (8), which instead predicts a ratio as detailed in equation (9). Similar observations regarding the Crank model were reported by Jiokap Nono et al. [15] while modeling the drying kinetics of okra.

$$\text{For} \quad t = 0, \frac{Y_0}{Y_\infty} \approx 1 - \frac{8}{\pi^2} = 1 - 0.811 = 0.189 \neq 0 \tag{9}$$

With Y_0, the initial concentration of the diffusing material.

This indicates that the model (8) overestimates the value of Y_0, unlike equation (7), which correctly predicts a zero value for Y at the initial moment. Indeed, at t = 0, higher-order terms are not negligible, and we obtain equation (10), from equation (7):

$$\frac{Y_0}{Y_\infty} = 1 - \frac{8}{\pi^2} \cdot \sum_{n=0}^{\infty} \frac{1}{(2n+1)^2} \tag{10}$$

At $t = 0$, the exponential terms $\exp\left(- (2n+1)^2 \cdot \frac{\pi^2 \cdot D_e}{4 \cdot L_C^2} \cdot t \right)$ for all n values equal 1, because $\exp(0) = 1$. Using known results from series theory, namely the Fourier series of a square wave and the results from the Basel problem directly related to this series (results giving the sum of the series for the reciprocals of the squares of all positive integers), and mathematical analysis, the full series sum at $t = 0$ is given as in equation (11) [26]:

$$\sum_{n=0}^{\infty} \frac{1}{(2n+1)^2} = \frac{\pi^2}{8} \tag{11}$$

Therefore, equation (10) becomes equation (12), which respects the initial conditions:

$$\frac{Y_0}{Y_\infty} = 1 - \frac{8}{\pi^2} \cdot \frac{\pi^2}{8} = 1 - 1 = 0 \tag{12}$$

The first term of the Crank's analytical solution was used to estimate WL and SG rates and to evaluate the diffusion coefficients.

2.4.2. Modified Crank models (present work)

The simplification of Crank's analytical solution for long-time processes, represented by the first term of the series, is not suitable for fitting the entire kinetic curve. Furthermore, using the full series solution for the initial time could be computationally intensive. To avoid managing two separate models for the entire kinetics one for the initial moment and another for long times, and to maintain a simplified model that respects the initial conditions of the kinetics, we proceeded as follows, starting with Crank's simplified model for long kinetic times.

At time $t = 0$, the WL and the SG should both be equal to zero because, at this instant, the biological material is not yet in contact with the hypertonic solution. In other words, at $t = 0$ no mass transfer takes place. Despite the finite dimensions of the mango slices, which are parallelepipeds measuring $4 \times 1 \times 1$ cm^3, we assume they behave as a thin layer. Furthermore, in equation (9), the term $\frac{8}{\pi^2}$ is the constant for infinite media, meaning media with no special boundaries [27], and as seen in the previous section, this factor also limits the adjustment of the initial condition in the kinetics by Crank's simplified model for long time. This factor emerges to ensure that the diffusion solution adheres to the imposed initial and boundary conditions. It acts as a normalization factor, derived from the Fourier series expansion in diffusion problems, guaranteeing that the solution respects the initial conditions and the physical characteristics of the system. Consequently, we modify Crank's model in two different ways, resulting in two modified Crank models, to improve the fit of the original model across the entire time range of the kinetics:

1) First, we replace the parameter $\frac{8}{\pi^2}$ with a constant, which we call C_z, to be determined through modeling. This gives the Modified Crank Model I, whose expression is provided in equation (13). The parameter C_z is considered a shape correction factor, given that the system is not truly a thin layer.

$$\frac{Y}{Y_\infty} = 1 - C_z \cdot \exp(-k \cdot t) \tag{13}$$

$$\text{With} \quad k = \frac{\pi^2 \cdot D_e}{4 \cdot L_c^2} \tag{14}$$

where C_z is a non-dimensional constant that reflects experimental data more accurately across the entire drying process, because C_z is adjusted based on fitting the model to the experimental data. k is the diffusion kinetics constant, in min^{-1}.

2) Secondly, we addressed the overestimation of the initial dependent value in the simplified Crank model by rounding the value of $\frac{8}{\pi^2}$ to 1, ensuring that at $t = 0$, $Y = 0$. This leads to the Modified Crank II model, whose expression is given by equation (15).

$$\frac{Y}{Y_\infty} = 1 - \exp(-k \cdot t) \tag{15}$$

The rearrangement of equations (13) and (15) is given by equations (16) and (17) respectively.

$$\ln\left(\frac{Y_\infty - Y}{Y_\infty}\right) = \ln C_z - \left(\frac{\pi^2 \cdot D_e}{4 \cdot L_C^2}\right) \cdot t \tag{16}$$

$$\ln\left(\frac{Y_\infty - Y}{Y_\infty}\right) = - \left(\frac{\pi^2 \cdot D_e}{4 \cdot L_C^2}\right) \cdot t \tag{17}$$

These two models were thus adjusted to improve accuracy across the entire drying process by estimating the model parameters from the experimental data. The kinetics data were modeled using MATLAB R2019 software. Validation of these models would allow the predictions throughout the dehydration process, rather than switching between different models for initial and later times.

2.4.3. Azuara model (1992)

Azuara et al. [28] modeled water loss and solute gain during D2I from material balances, obtaining equations that require two adjustable parameters [28]. A mass balance for water during D2I is given by:

$$WL = WL_{\infty} - M_w \tag{18}$$

M_w is the mass of water that can diffuse but remains inside the fruit at time t for a constant temperature and concentration of hypertonic solution. Water loss is a function of the amount of water that can diffuse, M_w, and the time t:

$$WL = s_w \cdot t \cdot M_w \tag{19}$$

Substituting equation (18) into equation. (19) followed by some rearrangement leads to equation (20a):

$$WL = \frac{s_w \cdot t \cdot WL_{\infty}}{1 + s_w \cdot t} \tag{20a}$$

Similarly, equation (20b) is obtained for the solute gain SG:

$$SG = \frac{s_s \cdot t \cdot SG_{\infty}}{1 + s_s \cdot t} \tag{20b}$$

where sw and ss are parameters that can be defined as relative rate constants for water loss and solute gain respectively.

The main advantage of the Azuara model is its ability to predict the equilibrium value. As with many other models, the disadvantage of Azuara's model is that it does not take into account the size, shape or structure of the material.

2.4.4. Weibull distribution model

The Weibull model concerns probability distribution functions used to describe the behavior of complex processes with a certain degree of variability [29], such as the D2I process [30]. The fractional amount of water loss and solute gain during the D2I process is presented in Equation (21).

$$\frac{Y}{Y_{\infty}} = 1 - \exp\left(-\left(\frac{t}{\alpha}\right)^{\beta}\right) \tag{21}$$

α is the scale parameter of the Weibull's model for water loss (α_w) or solute gain (α_s) that is associated with the process rate when the process time equals α, the ratio $\frac{Y}{Y_{\infty}}$ value is $\left(1 - \frac{1}{e}\right)$. β is the shape parameter for water loss (β_w) or solute gain (β_s).

2.5. Determination of diffusion coefficient and activation energy

The diffusion coefficient of water (D_{ew} in $m^2 \cdot s^{-1}$) and solute (D_{es} in $m^2 \cdot s^{-1}$) in mango slices was determined using either the diffusion coefficient predicted by the Crank, Modified Crank I, or Modified Crank II models. The activation energies were determined using the Arrhenius equation expressed by Equation (22):

$$D_e = D_0 \exp\left(\frac{-E_a}{R \cdot T}\right) \tag{22}$$

where D_0 is the Arrhenius factor, $m^2 \cdot s^{-1}$, generally defined as the reference diffusion coefficient at an infinitely high temperature, E_a is the activation energy of diffusion, $J \cdot mol^{-1}$, R is the universal gas constant, $J \cdot mol^{-1} \cdot K^{-1}$, T is the temperature, K.

The linearization of equation (22) is presented in equation (23):

$$-\ln(D_e) = -\ln(D_0) + \frac{E_a}{R} \cdot \frac{1}{T} \tag{23}$$

The activation energy, E_a, is therefore easily calculated using the slope, $\frac{E_a}{R}$, of the curve $-\ln(D_e) = f\left(\frac{1}{T}\right)$. The software used to determine the activation energy is MATLAB R2019a.

2.6. Statistical analysis and model validation

The models were evaluated using validation criteria such as the coefficient of determination, the adjusted coefficient of determination, the root mean square error, and the mean relative error, whose formulas are presented in equations (24)–(27), respectively:

$$R^2 = 1 - \frac{\sum_{i=1}^{N}\left(y_{(i,exp)} - y_{(i,calc)}\right)^2}{\sum_{i=1}^{N}\left(y_{(i,exp)} - \overline{y}_{(i,exp)}\right)^2} \tag{24}$$

$$R^2_{adj} = 1 - \frac{(1 - R^2)\cdot n - 1}{n - p} \tag{25}$$

$$RMSE = \left(\frac{\sum_{i=1}^{N}\left(y_{i,calc} - y_{i,exp}\right)^2}{n}\right)^{1/2} \tag{26}$$

$$MRE = \frac{1}{n}\frac{\sum_{i=1}^{N}\left|y_{i,calc} - y_{i,exp}\right|}{y_{i,exp}} \tag{27}$$

With R^2: coefficient of determination; R^2_{adj}: adjusted coefficient of determination; RMSE: square root of the mean error; MRE: mean relative error; $y_{i,exp}$: experimental WL or SG; $y_{i,calc}$: predicted WL or SG response; p: number of constants and n the number of observations.

In order to find the most representative model for the study, the models were ranked according to the minimum sum ranking criterion (Σmin), which is the sum of the average validation criteria. The equation for this criterion for selecting the best model is a function of the mean of each model validation criteria, the mathematical expression of which is presented by equation (28):

$$\sum \min = (1 - \overline{R^2}) + \left(1 - \overline{R^2_{adj}}\right) + \overline{RMSE} + \overline{MRE} \tag{28}$$

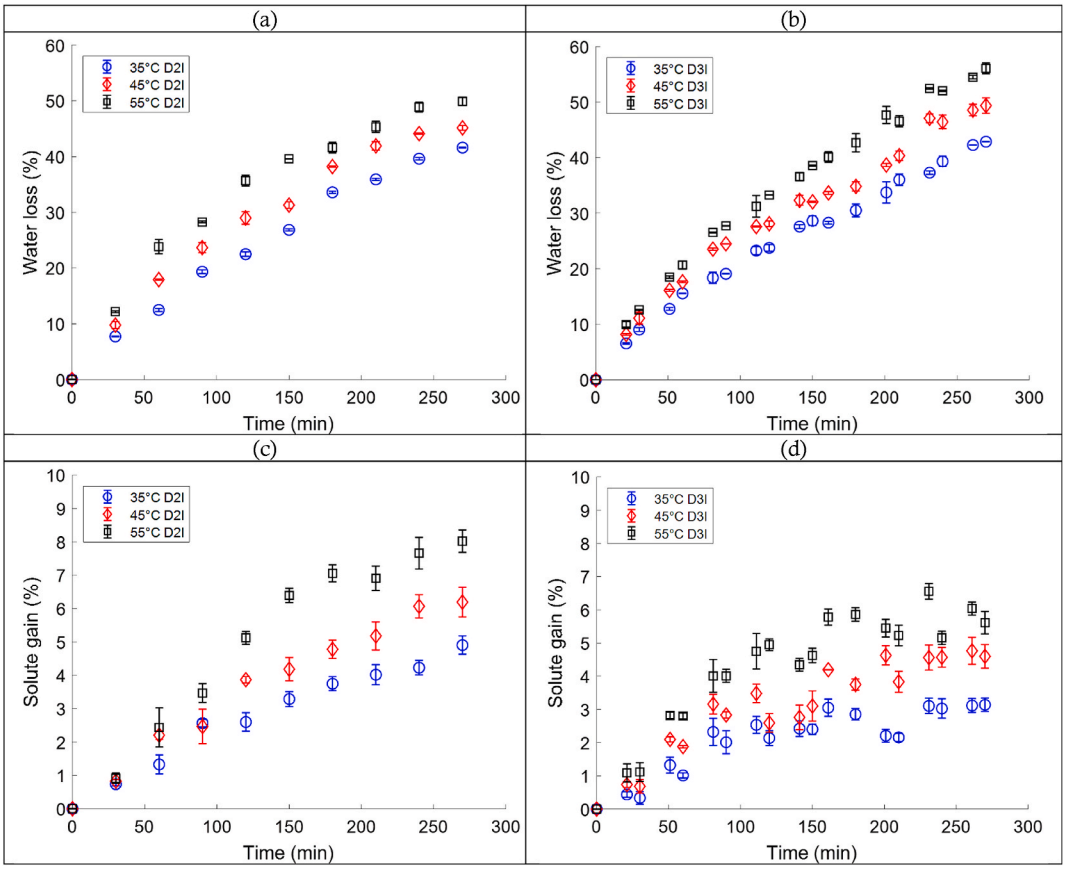

Fig. 4. Scatter plot of experimental data showing the evolution of water loss and solute gain as a function of time and temperature (35, 45, and 55 °C), for D2I (a,c) and D3I (b,d), with error bars representing the standard deviation.

3. Results and discussion

3.1. Effect of intermittency on mass transfer during osmotic dehydration

Fig. 4 illustrates the experimental evolution of WL and SG as a function of time and temperature during D2I (Fig. 4 (a) and 4 (c)) and D3I (Fig. 4 (b) and 4 (d)) respectively. The results of Ayetigbo et al. [23]; Kaur et al. [31] and Zongo et al. [32] demonstrate the increase of WL and SG with time and temperature during osmotic dehydration of mango slices and are consistent with our observations that WL and SG increase with increasing time and temperature as depicted in Fig. 4. Mass transfer occurs during the first stages of the D2I and D3I processes. However, as the hypertonic solution gains water, the difference in osmotic pressures between the product and solution is smaller, which slows down the mass transfer rate till equilibrium [1,32]. It's worth noting that tissue contraction of the product may occur simultaneously with the dehydration process, reducing the physical space in which mass transfer may occur [33].

We observe that the more biological material is immersed in a hypertonic solution, the more water it loses through the combined phenomena of osmosis and diffusion, while simultaneously becoming impregnated with solute through mass diffusion. Additionally, we note that the processes of dehydration and impregnation accelerate with increasing temperature. Indeed, when the temperature rises the permeability of the cells increases, increasing the fragility of the biological matrix's fibrous and cellular structure. Additionally, the solubility of the solute increases and the hypertonic solution's viscosity decreases, enhancing the mass transfer of water loss and solute gain [34–37]. To better understand and read the curves, as well as to establish a more meaningful comparison between D2I and D3I, a modeling study of these experimental points was conducted using the Azuara model, the Weibull model, the Crank model, and the two modified Crank models developed in this work.

3.2. Modeling of mass transfer kinetics during D2I and D3I

Figs. 5–9 depict the results of modeling WL and SG kinetics as a function of temperature during D2I and D3I. Each figure shows the experimental points and the modeling curves. The validation parameters for each model are shown in Table 1. Overall, like the experimental points for WL and SG, the curves for the different models increase with time and temperature. A visual observation of

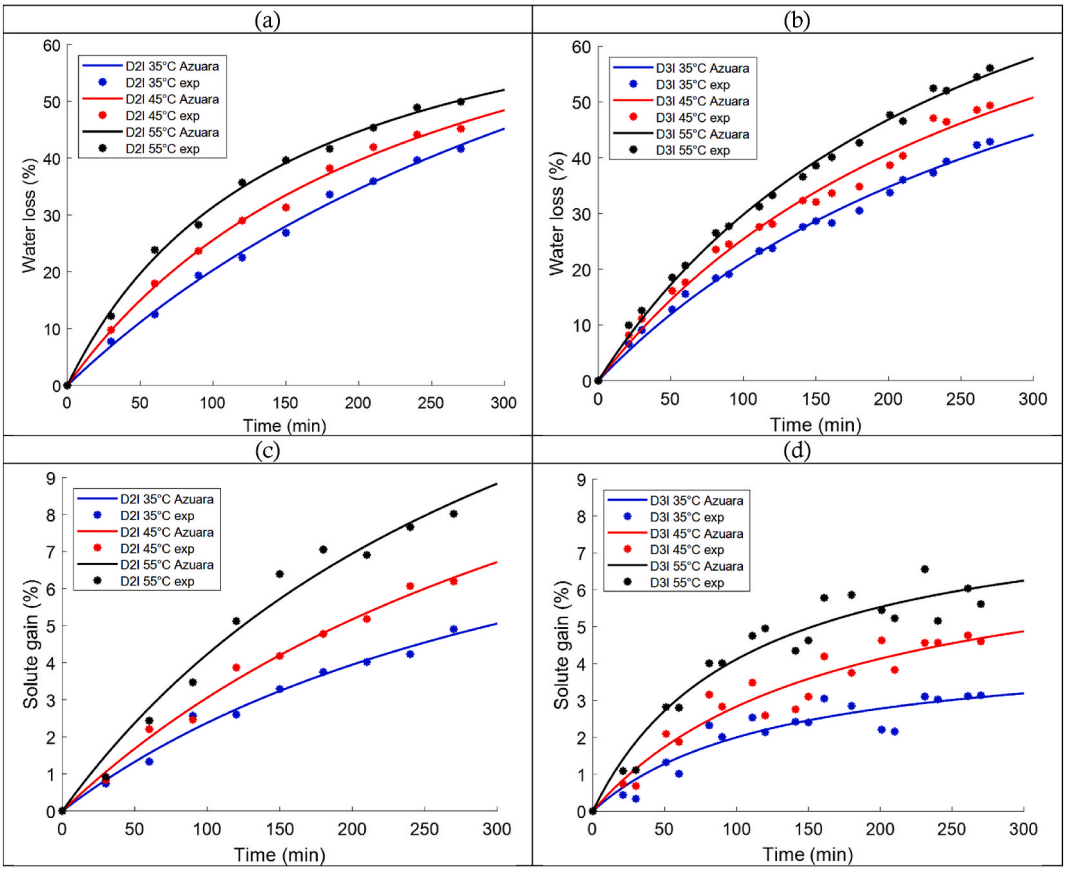

Fig. 5. Water loss (WL) and solute gain (SG) as a function of time and temperature (35, 45, and 55 °C): Experimental points (*) and corresponding predicted curves from the Azuara model (solid lines) for D2I (a,c) and D3I (b,d).

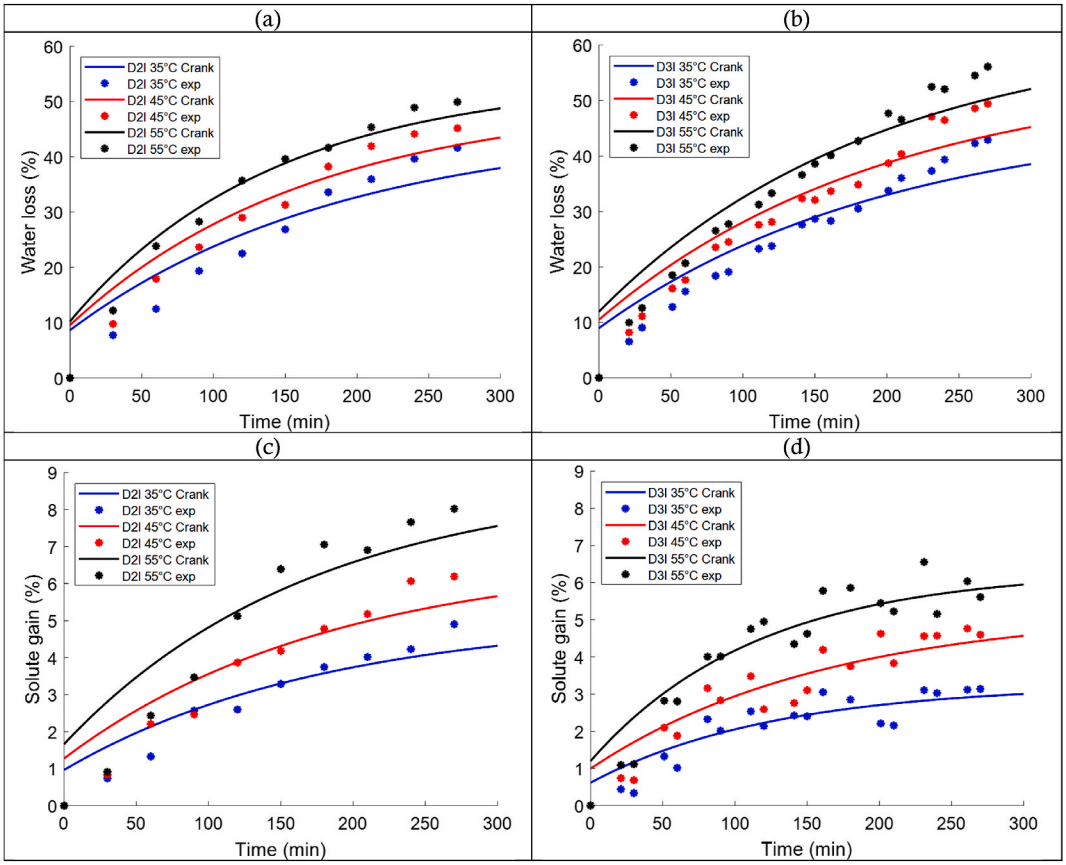

Fig. 6. Water loss (WL) and solute gain (SG) as a function of time and temperature (35, 45, and 55 °C): Experimental points (*) and corresponding predicted curves from the Crank model (solid lines) for D2I (a,c) and D3I (b,d).

Figs. 5–9 shows that the curves predicted by the Crank models do not start at the origin, and therefore deviate from the theory according to which, at the initial instant, water loss and solute gain are zero. Among the models, only the Modified Crank I model passes through the origin when considering D2I water loss kinetics.

The other models, namely the Azuara, Modified Crank II, and Weibull models, faithfully predict water loss and solute gain at the initial instant. Using statistical validation criteria, we can make a numerical assessment of which models best predict WL and SG kinetics during D2I and D3I. Table 1 gives a classification of the different models.

From Tables 1 and 2, it is visible that the Weibull model and the Modified Crank II model are the models that best describe both the mass transfer process during D2I and D3I. Furthermore, we observe that the Modified Crank I model ranks third, with a value of Σmin close to that of the Modified Crank II model in both D2I and D3I processes. This allows us to conclude that the Modified Crank I model can also be used to fit the experimental points in the osmotic dehydration process. However, as shown in Fig. 7, the curves of the model do not always start from the origin, which is a drawback.

Tables 3 and 4 show the parameter values of all models, for WL and SG, as a function of temperature and immersion mode. Out of the best models validated above (Modified Crank II and Weibull), we note that the Weibull model provides outlier values of equilibrium water loss (WL_∞) for D3I, with values ranging from 226.9 to 4043 %. As a result, we choose the Modified Crank II model as the best model for predicting the WL_∞. This value is critical in calculating the diffusion coefficient.

Table 3 shows that WL_∞ decreases with temperature during D2I and increases with temperature during D3I. In Table 4 we note that, during D2I, the SG_∞ increasing with increasing temperature. It could be argued that continuous immersion is the cause of this decrease in WL_∞ with increasing temperature during D2I. The longer the immersion, the more solute seeps into the pores of the biological material, which consequently slows down the dehydration process. The higher the temperature, the faster the solute seeps into the pores of the biological material, reducing the time required to attain thermodynamic equilibrium, which explains why WL_∞ decreases with increasing temperature. These findings are consistent with those of Sablani and Rahman [38] who demonstrated that WL_∞ decreases with increasing temperature while equilibrium solute gain (SG_∞) increases with temperature regardless of mango geometric shape.

In the case of D3I, we noted an increase in WL_∞ with an increase in temperature (Table 3). This can be attributed to the intermittent immersion process, as halting immersion not only interrupts the infiltration of the solute but also allows the solute found in the pores and on the material's surface to be released due to the escape of water molecules. Thus, the higher the temperature, the faster this

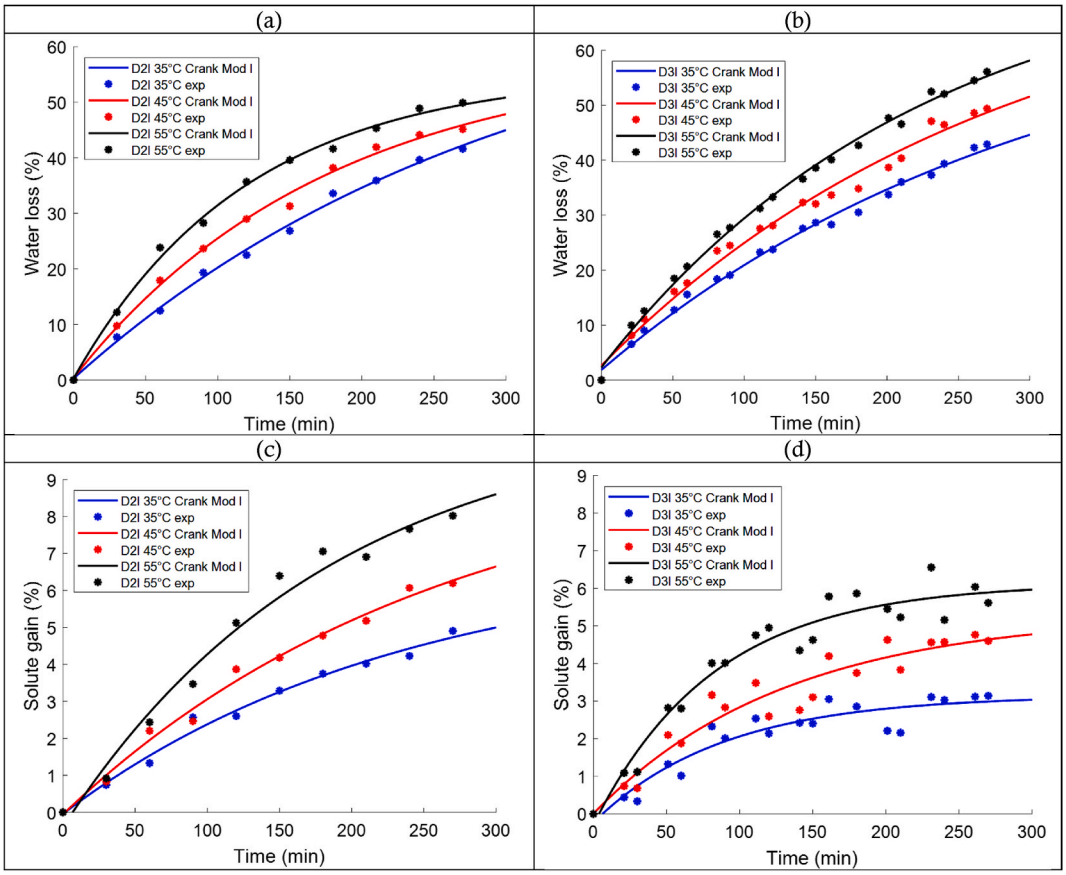

Fig. 7. Water loss (WL) and solute gain (SG) as a function of time and temperature (35, 45, and 55 °C): Experimental points (*) and corresponding predicted curves from the Modified Crank I model (solid lines) for D2I (a,c) and D3I (b,d).

process will be, limiting the pore-clogging process and increasing the time required to reach thermodynamic equilibrium. This is why WL_∞ increases with temperature. We can accept the hypothesis that during de-immersion there is the possibility of dehydration of slices in the mango and that the higher the temperature of the D3I operation, the more noticeable the phenomenon of dehydration will be. We can conclude that this phenomenon can contribute greatly to the increase in WL during D3I.

The equilibrium solute gain, SG_∞, increases with temperature during D2I and D3I as shown in Table 4. This is because temperature significantly increases the material's pore size and cellular permeability, thus facilitating the infiltration of the solute into the material. Whatever the temperature, D3I has a lower SG than D2I. This observation could be explained by the fact that during intermittence, there is competition between water exiting and solute entering the biological matrix, with water loss dominating, thereby slowing the progress of the solute within the porous structure of the material.

In Fig. 8 (c) and 8 (d), the solute gain kinetics in D3I quickly reaches a pseudo-equilibrium for a low solute gain value, compared to that of D2I. This low pseudo-equilibrium value could be attributed to the material's recurrent de-immersion during the process, causing a drive of the solute towards the outside, which is transported by water and materialized by the elimination of the film of hypertonic solution on the material's surface.

In contrast, in Fig. 8 (a) and 8 (b), the kinetics of water loss reaches a pseudo plateau more quickly in D2I than in D3I. In other words, D2I achieves thermodynamic equilibrium faster than D3I, implying that, for long kinetic times, D2I process is less effective than D3I process. This indicates that the D3I process leads to a slower saturation of the biological material's pores with solute compared to the D2I process.

3.3. *Diffusion coefficient and activation energy*

The Modified Crank II model was used to determine the water and solute diffusion coefficients, as it is the only model selected for the study that best predicts the values of WL_∞ and SG_∞ in both D2I and D3I. Equations (15) and (17) outline the expression for the Modified Crank II model and its rearrangement equation. The values of the predicted water and solute diffusion coefficients and the values of the model validation criteria are presented in Table 5.

Table 5 shows the evolution of water and solute diffusion coefficients as a function of temperature and we realize that the water and

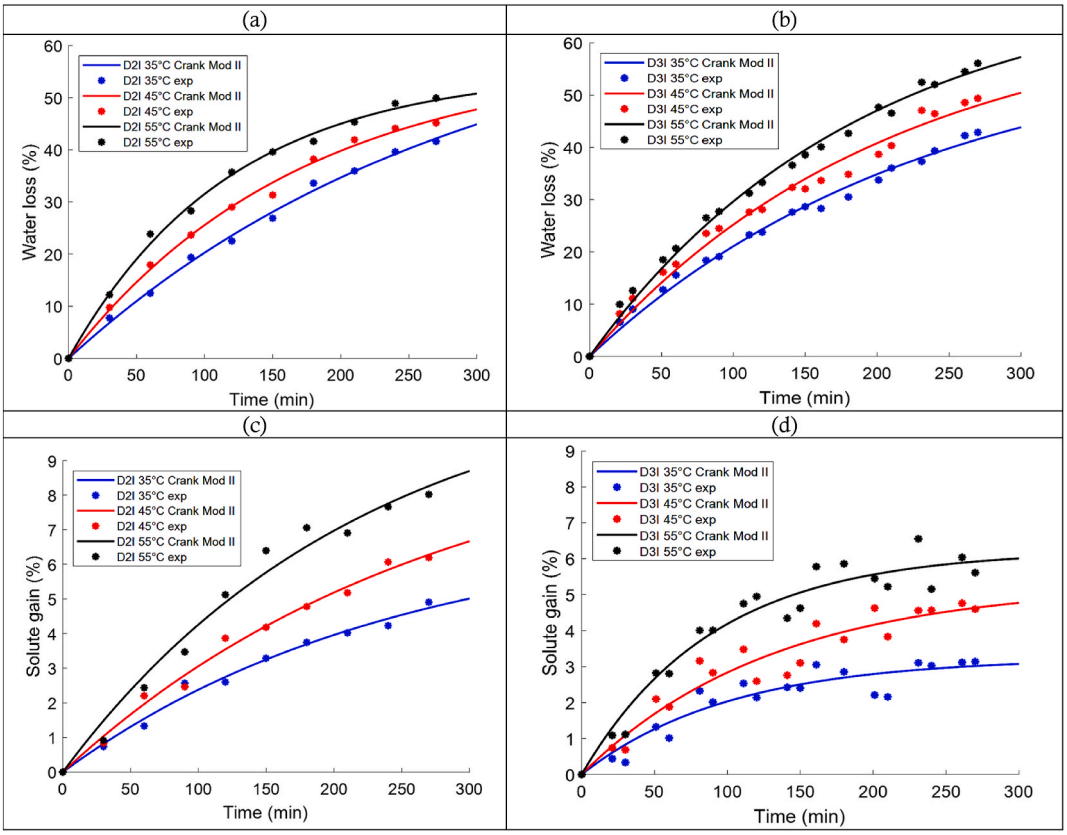

Fig. 8. Water loss (WL) and solute gain (SG) as a function of time and temperature (35, 45, and 55 °C): Experimental points (*) and corresponding predicted curves from the Modified Crank II model (solid lines) for D2I (a,c) and D3I (b,d).

solute diffusion coefficients increase with temperature in both D2I and D3I. This observation parallels the findings of Alakali et al. [39] on the kinetics of osmotic dehydration of mango, which similarly demonstrated an increase in the diffusion coefficients of water and solute with temperature.

Solute diffusion coefficients are higher in D3I than in D2I. Indeed, the time constants of the process are greater in D2I than in D3I. However, the diffusion coefficient is proportional to the dehydration rate constant, itself inversely proportional to the time constant of the process. Taking into account the results presented in Fig. 8, the slopes at the origin show that the solute diffuses very quickly at the start of the D3I, and quickly reaches a pseudo equilibrium at low values of the solute gain, compared to that of the D2I, linked to the process of repeated de-immersion of the material. Regarding water loss, we obtain higher water coefficient values in D2I compared to D3I. In contrast to the solute transfer kinetics, Fig. 8 shows that water losses have smaller time constants in D2I than in D3I. This greater diffusion of water in D2I would be due to the continuous immersion of the material during the process. However, D3I presents water diffusion coefficient values comparable to those of D2I, for low temperatures, between 35 and 45 °C. The review of Asghari et al. [40] highlighted the advantage of implementing osmotic dehydration techniques at temperatures close to ambient temperature, it appears that at low temperatures, it is D3I which is advantageous compared to D2I. Additionally, over time, D2I reaches its plateau very quickly, compared to D3I which continues to grow.

The values of the diffusion coefficients obtained allowed us to determine the activation energy (E_a) and Arrhenius factor during the dehydration and impregnation process. The activation energy is a measure of the dependence of the mass transfer process on temperature and a larger magnitude of E_a is associated with higher temperature dependence. Table 6 presents the values of the predicted activation energies, the Arrhenius factors, and the values of the validation criteria. The D2I process exhibits higher activation energies for WL and SG, respectively, compared to those obtained in D3I, indicating that the mass transfers in D2I are more sensitive to temperature changes than those in D3I [39].

At the end of this study, it is essential to highlight that the primary challenge in osmotic dehydration (D2I) of fruits is to dehydrate them while preserving their original characteristics, particularly their sugar content. This challenge is particularly complex due to the unavoidable sugar impregnation that occurs during the process. The solution often involves minimizing this impregnation, which is achieved with the new dehydration process (D3I) that we have developed [8]. This innovative process allows for the osmotic treatment of products while significantly reducing their sugar content [8].

Economically, by lowering the solute gain (reduced sugar impregnation in the fruits), this process reduces costs related to supplementing the concentrated solution to maintain a constant concentration. This allows manufacturers to offer reduced-sugar products

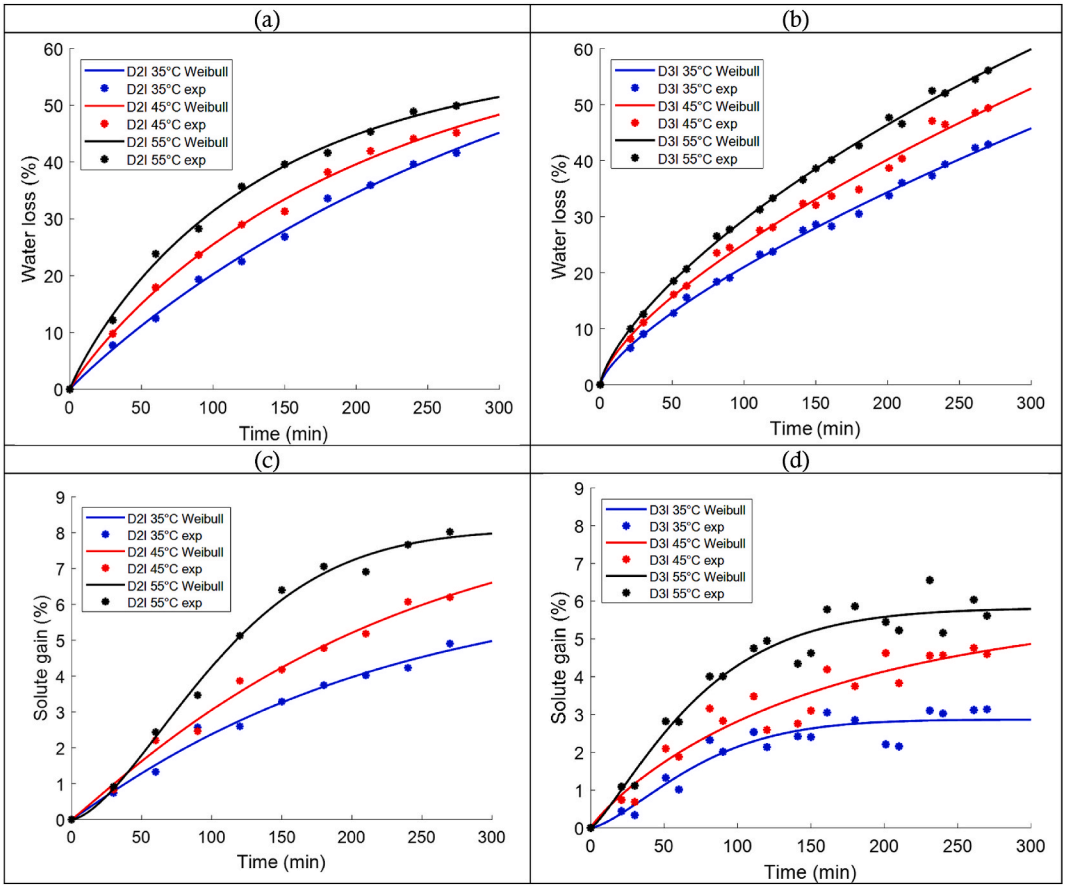

Fig. 9. Water loss (WL) and solute gain (SG) as a function of time and temperature (35, 45, and 55 °C): Experimental points (*) and corresponding predicted curves from the Weibull model (solid lines) for D2I (a,c) and D3I (b,d).

Table 1
Classification of models for water loss (WL) kinetics in D2I and D3I, based on Σmin values.

Models	WL (D2I)					Models	WL (D3I)				
	$\overline{R^2}$	$\overline{R^2_{adj}}$	$\overline{RMSE}$	$\overline{MRE}$	Σmin		$\overline{R^2}$	$\overline{R^2_{adj}}$	$\overline{RMSE}$	$\overline{MRE}$	Σmin
Modified Crank II	0.996	0.996	0.975	0.028	1.011	Weibull	0.996	0.996	0.887	0.022	0.917
Weibull	0.996	0.995	1.020	0.027	1.055	Modified Crank II	0.992	0.991	1.266	0.033	1.315
Modified Crank I	0.996	0.995	1.032	0.027	1.067	Azuara	0.991	0.991	1.303	0.081	1.402
Azuara	0.996	0.996	0.970	0.090	1.067	Modified Crank I	0.990	0.989	1.419	0.054	1.494
Crank	0.902	0.889	5.272	0.144	5.624	Crank	0.899	0.893	4.389	0.154	4.751

Table 2
Classification of models for solute gain (SG) kinetics in D2I and D3I, based on Σmin values.

Models	SG (D2I)					Models	SG (D3I)				
	$\overline{R^2}$	$\overline{R^2_{adj}}$	$\overline{RMSE}$	$\overline{MRE}$	Σmin		$\overline{R^2}$	$\overline{R^2_{adj}}$	$\overline{RMSE}$	$\overline{MRE}$	Σmin
Weibull	0.990	0.988	0.217	0.052	0.291	Weibull	0.924	0.914	0.369	0.128	0.659
Modified Crank II	0.990	0.988	0.217	0.052	0.291	Modified Crank II	0.920	0.910	0.377	0.132	0.678
Modified Crank I	0.987	0.983	0.218	0.070	0.318	Modified Crank I	0.918	0.913	0.370	0.145	0.683
Azuara	0.985	0.983	0.205	0.203	0.440	Azuara	0.914	0.909	0.374	0.203	0.753
Crank	0.860	0.843	0.697	0.270	1.264	Crank	0.853	0.844	0.482	0.239	1.024

Table 3
Fitting parameters for water loss (WL) as a function of temperature and pre-treatment (D2I or D3I).

	Models	Azuara		Crank		Modified Crank I			Modified Crank II		Weibull		
	Coef	WL_∞ (%)	$s_w \times 10^{-3}$ (min^{-1})	WL_∞ (%)	$k_{WL} \times 10^{-3}$ (min^{-1})	WL_∞ (%)	C_{zw}	$k_{WL} \times 10^{-3}$ (min^{-1})	WL_∞ (%)	$k_{WL} \times 10^{-3}$ (min^{-1})	WL_∞ (%)	α_w (min)	β_w
D2I	35 °C	116.96	2.10	45.58	5.27	71.76	1.00	3.27	70.06	3.41	78.61	353.40	0.71
	45 °C	87.54	4.13	50.36	5.93	58.50	0.99	5.66	57.78	5.84	64.73	212.16	0.68
	55 °C	77.45	6.82	54.00	7.07	55.33	0.99	8.36	55.11	8.48	58.82	134.73	0.72
D3I	35 °C	96.10	2.83	47.23	4.94	70.51	0.97	3.25	60.84	4.25	2603.54	86001.06	0.71
	45 °C	101.57	3.34	55.22	4.99	77.33	0.97	3.55	66.10	4.81	4042.99	173554.99	0.68
	55 °C	109.55	3.74	62.87	5.17	78.49	0.97	4.40	71.83	5.33	226.93	1547.94	0.72

Coef: Coefficient.

Table 4
Fitting parameters for solute gain (SG) as a function of temperature and pre-treatment (D2I or D3I).

	Models	Azuara		Crank		Modified Crank I			Modified Crank II		Weibull		
	Coef	SG_∞ (%)	$s_s \times 10^{-3}$ (min^{-1})	SG_∞ (%)	$k_{SG} \times 10^{-3}$ (min^{-1})	SG_∞ (%)	C_{zw}	$k_{SG} \times 10^{-3}$ (min^{-1})	SG_∞ (%)	$k_{SG} \times 10^{-3}$ (min^{-1})	SG_∞ (%)	α_s (min)	β_s
D2I	35 °C	11.56	2.59	5.11	5.53	6.95	1.01	4.26	7.10	4.08	6.57	215.24	1.04
	45 °C	16.73	2.24	6.74	5.41	9.80	1.01	3.80	10.07	3.62	8.95	227.93	1.06
	55 °C	19.38	2.79	8.79	5.84	10.85	1.04	5.37	11.74	4.50	8.09	120.37	1.57
D3I	35 °C	4.55	7.84	3.25	7.86	3.15	1.07	11.34	3.24	9.86	2.87	80.17	1.45
	45 °C	7.62	5.93	5.24	6.14	5.32	1.00	7.61	5.31	7.65	5.92	163.05	0.89
	55 °C	8.43	9.53	6.33	8.67	6.13	1.05	12.13	6.23	11.17	5.82	79.07	1.25

Coef: Coefficient.

Table 5
Modified Crank II diffusion coefficients and values of validation statistical criteria at 35 °C, 45 °C, and 55 °C.

		Temperature		
		35 °C	45 °C	55 °C
D2I	D_{ew} ($m^2 \cdot s^{-1}$)	5.76×10^{-10}	9.87×10^{-10}	1.45×10^{-9}
	R^2	0.99	0.99	0.99
	R^2_{adj}	0.99	0.99	0.99
	RMSE	0.02	0.05	0.07
	D_{es} ($m^2 \cdot s^{-1}$)	6.79×10^{-10}	7.16×10^{-10}	8.43×10^{-10}
	R^2	0.99	0.99	0.98
	R^2_{adj}	0.99	0.99	0.98
	RMSE	0.05	0.04	0.07
D3I	D_{ew} ($m^2 \cdot s^{-1}$)	7.22×10^{-10}	8.19×10^{-10}	9.05×10^{-10}
	R^2	0.99	0.98	0.99
	R^2_{adj}	0.99	0.98	0.99
	RMSE	0.04	0.06	0.04
	D_{es} ($m^2 \cdot s^{-1}$)	1.29×10^{-9}	1.34×10^{-9}	1.54×10^{-9}
	R^2	0.79	0.89	0.69
	R^2_{adj}	0.79	0.89	0.69
	RMSE	0.31	0.24	0.48

Table 6
Values of activation energies, Arrhenius factors, and model validation statistical criteria for water loss (WL) and solute gain (SG) of mango slices, pre-treated with D2I or D3I.

Coefficients	WL		SG	
	D2I	D3I	D2I	D3I
D_0 ($m^2 \cdot s^{-1}$)	2.21×10^{-3}	2.96×10^{-8}	2.29×10^{-9}	2.21×10^{-8}
E_a ($J \cdot mol^{-1}$)	38789	9503	9037	7327
R^2	0.99	0.99	0.91	0.89
R^2_{adj}	0.99	0.99	0.91	0.89
RMSE	0.05	0.01	0.03	0.03

to the market at lower costs. Such products address the growing consumer demand for healthier food options and help prevent health issues associated with excessive sugar consumption, including obesity, type 2 diabetes, cardiovascular diseases, and dental cavities as mentioned by Erickson and Carr in 2020 [41]. By offering reduced-sugar products, companies can promote public health while positioning themselves advantageously in a growing market. Furthermore, the calculated activation energies revealed that the D3I process is less temperature-sensitive than the D2I process.

4. Conclusion

The water loss (WL) and solute gain (SG) kinetics followed by modeling allowed us to compare the behavior of the mango slices during D2I and D3I. Semi-empirical modeling allowed to observe that the equilibrium water loss decreases with increasing temperature during D2I and increases with temperature during D3I. On the other hand, the equilibrium solute gain during D2I and D3I increases with temperature but is higher in D2I than in D3I. Modified Crank II was the best model to describe the behavior of WL and SG during D2I and D3I, and was used to estimate the apparent diffusion coefficient. The average water diffusion coefficient was between (3.46 and 8.69) $\times 10^{-8}$ m^2 s^{-1} for D2I and (4.33 and 5.43) $\times 10^{-8}$ m^2 s^{-1} for D3I. The solute diffusion coefficient was between

(4.07 and 5.06) $\times 10^{-8}$ m^2 s^{-1} for D2I and (7.74 and 9.23) $\times 10^{-8}$ m^2 s^{-1} for D3I. The activation energies of water and solute were higher in D2I than in D3I. We demonstrate that intermittency enhances mass transfer during osmotic dehydration of mango slices. The results of modeling mass transfers obtained in this work indicate that the new technique developed by D3I opens new avenues for exploring the osmotic dehydration of fruits and vegetables. The low-temperature dependence of transfers, and the low solute gains observed in the D3I process compared to the conventional D2I process, offer a clear economic advantage. It aligns with our goal of achieving healthier product outcomes. However, several limitations need to be addressed. Firstly, the sample size and variability of the fruits may significantly influence the accuracy of the mathematical model used. Secondly, the impact of the process on other nutritional or sensory attributes of the fruits was not thoroughly investigated and could also be modeled. Future research should address these limitations by testing a broader range of fruit varieties, optimizing the process under different conditions, and exploring how other nutrients and other operating conditions affect the models. These studies could offer valuable insights into the broader implications of this new process.

CRediT authorship contribution statement

C. Tsopwo Zena: Writing – original draft, Resources, Methodology, Investigation, Formal analysis, Data curation. **Y. Jiokap Nono:** Writing – review & editing, Writing – original draft, Visualization, Validation, Supervision, Resources, Project administration, Investigation, Funding acquisition, Formal analysis, Data curation, Conceptualization.

Statement for acceptance of the publication of this work

- All the authors approve the publication of this work.
- The head of the LASE (Laboratoire d'Analyses, Simulation et Essais) at the University Institute of Technology (IUT) of the University of Ngaoundere, and the head of the LARESH (Laboratoire de Réaction, Extraction, Séchage, Sucrerie et Huilerie) at the National Advanced School of Agro-Industrial Sciences (ENSAI), of the University of Ngaoundere, where the work was carried out, approve the publication of this work.

Data availability statement

- Data associated with our study were not deposited into a publicly available repository.
- The data are included in the article and are accessible to the public. Further information will be made available upon request.

Animal and human experiments

The present work doesn't include animal or human experiments.

Funding

This research was not funded. Concerning the publication procedure, the authors are supported by Heliyon which covers 100 % of the APC: the corresponding author and the coauthor are all from a Group A country: Cameroon.

Declaration of competing interest

The authors declare that they have no known competing financial interests or personal relationships that could have appeared to influence the work reported in this paper.

Acknowledgements

The authors gratefully acknowledge the financial support from the Ministry of Higher Education of Cameroon through the Special Fund Account for the modernization of research in state Universities (Presidential Decree No. 2009/121 of April 8, 2009).

References

[1] I. Ahmed, I.M. Qazi, S. Jamal, Developments in osmotic dehydration technique for the preservation of fruits and vegetables, Innovat. Food Sci. Emerg. Technol. 34 (2016) 29–43.
[2] Nono Y. Jiokap, M. Reynes, N. Zakhia, A.L. Raoult-Wack, F. F. Giroux, Mise au point d'un procédé combiné de déshydratation imprégnation par immersion et séchage de bananes (*Musa acuminata* groupe Cavendish), J. Food Eng. 55 (2002) 231–236.
[3] S. Chandra, D. Kumari, Recent development in osmotic dehydration of fruit and vegetables: a review, Crit. Rev. Food Sci. Nutr. 55 (4) (2015) 552–561.
[4] M. Akbarian, N. Ghasemkhani, F. Moayedi, Osmotic dehydration of fruits in food industrial: a review, Int. J. Biosci. 4 (1) (2014) 42–57.
[5] A.L. Raoult-Wack, G. Rios, S. Guilbert, Sucrose and osmotic dehydration, in: M. Mathlouthi, P. Reiser (Eds.), Sucrose, Springer, Boston, MA, 1995.
[6] A.K. Yadav, S.V. Singh, Osmotic dehydration of fruits and vegetables: a review, J. Food Sci. Technol. 51 (9) (2014) 1654–1673.
[7] D. Torreggiani, Osmotic dehydration in fruits and vegetable processing, Food Res. Int. 26 (1993) 59–68.

[8] Zena C. Tsopwo, Nono Y. Jiokap, Investigating intermittent immersion during osmotic dehydration of mango (*Mangifera indica* L. Moench). Part A: determination of optimal conditions for mango (*Mangifera indica* L. Moench) dehydration impregnation by immersion (D2I) and intermittent immersion (D3I), Heliyon 10 (3) (2024) e35808, https://doi.org/10.1016/j.heliyon.2024.e35808, 21pp.

[9] F.R. Assis, R.M. Morais, A.M. Morais, Mathematical modelling of osmotic dehydration kinetics of apple cubes, J. Food Process. Preserv. (2016) 16.

[10] J. Crank, The Mathematics of Diffusion, second ed., Clarendon Press Oxford, 1975, p. 421p.

[11] F.R. Assis, R.M. Morais, A.M. Morais, Mass transfer in osmotic dehydration of food products: comparison between mathematical models, Food Eng. Rev. 8 (2) (2015) 116–133.

[12] Oumarou Elhadji Moussa, I.L. Kouedjou, M. Tchotsoua, Mango production, a major stake for the development of the sector of the urban district of Ngaoundere III, in: Y. Jiokap Nono (Ed.), Proceedings of the LOREXP-2021 International Conference on "Value Chains and Integral Transformation of Local Resources", Ngaoundere-Cameroon, 20-23 April, 2021, pp. 260–274. REF: LOREXP_2021_A1216, https://lorexp.org/proceedings/, https://lorexp.org/wp-content/uploads/2021/11/13_LOREXP_2021_A1216_OUMAROU.pdf.

[13] A.L. Raoult-Wack, G. Rios, S. Guilbert, Sucrose and osmotic dehydration, in: M. Mathlouthi, P. Reiser (Eds.), Sucrose, Springer, Boston, MA, 1995, pp. 279–290.

[14] R. Klewicki, M. Uczciwek, Effect of osmotic dehydration in fructose, sucrose and fructooligosaccharide solutions on the content of saccharides in plums and apples and their energy value, Agric. Food Sci. 17 (4) (2008) 367–375.

[15] Y. Jiokap Nono, N. Telewo, N.L. Nanko, C. Kapseu, Study of the drying kinetics of okra (*Abelmoschus esculentus* L.): influence of disc size, drying temperature, pretreatment and variety, in: Y. Jiokap Nono (Ed.), Proceedings of the LOREXP-2021 International Conference on "Value Chains and Integral Transformation of Local Resources", Ngaoundere-Cameroon, 20-23 April, 2021, pp. 426–446. REF: LOREXP_2021_A1238, https://lorexp.org/proceedings/, https://lorexp.org/wp-content/uploads/2021/11/11_LOREXP_2021_A1238_TELEWO.pdf.

[16] I. Pavkov, M. Radojcin, Z. Stamenkovic, K. Kešelj, U. Tylewicz, P. Sipos, O. Ponjican, A. Sedlar, Effects of osmotic dehydration on the hot air drying of apricot halves: drying kinetics, mass transfer, and shrinkage, Processes 9 (2) (2021) 22p, https://doi.org/10.3390/pr9020202, 202.

[17] D. Ndapeu, E. Njeugna, B.S. Bistac, J.Y. Jean Yves Drean, M. Fogue, J.N. Foba, Experimental study of the drying kinetics of the coconut shells (*Nucifera*) of Cameroon, Mater. Sci. Appl. 4 (12) (2013) 822–830, https://doi.org/10.4236/msa.2013.412105.

[18] M. Popescu, P. Iancu, V. Plesu, C.S. Bildea, F.A. Manolache, Mathematical modeling of thin-layer drying kinetics of tomato peels: influence of drying temperature on the energy requirements and extracts quality, Foods 12 (20) (2023) 3883, https://doi.org/10.3390/foods12203883.

[19] K. Mugodo, T.S. Workneh, The kinetics of thin-layer drying and modelling for mango slices and the influence of differing hot-air drying methods on quality, Heliyon 7 (6) (2021) e07182, https://doi.org/10.1016/j.heliyon.2021.e07182.

[20] M.E. Cavalcanti-Mata, M.E. Duarte, M. Tolentino, F.A. Mendes, L. Batista, J.M. de Lima, A. Lúcio, A.P. Nascimento, R.D. Almeida, H.M. Lisboa, Drying kinetics of industrial pineapple waste: effective diffusivity and thermodynamic properties resulting from new mathematical models derived from the Fick equation, Processes 12 (6) (2024) 1198, https://doi.org/10.3390/pr12061198.

[21] F.R. Assis, R.M. de Morais, A.M. de Morais, Mathematical modelling of the osmotic dehydration of physalis, Braz. J. Food Technol. 21 (2018) e2017102, 5.

[22] D. Dimakopoulou-Papazoglou, E. Katsanidis, Osmotic processing of meat: mathematical modeling and quality parameters, Food Eng. Rev. n°1 (2019) 32–47, https://doi.org/10.1007/s12393-019-09203-1.

[23] O. Ayetigbo, S. Latif, A. Abass, J. Müller, Osmotic dehydration kinetics of biofortified yellow-flesh cassava in contrast to white-flesh cassava (Manihot esculenta), J. Food Sci. Technol. 56 (9) (2019) 4251–4265, https://doi.org/10.1007/s13197-019-03895-3.

[24] van M. Boudewijn, P. Bons, B.A. Carreras, R. Sanchez, On the applicability of Fick's Law to diffusion in inhomogeneous systems, Eur. J. Phys. 26 (5) (2005) 913–925, https://doi.org/10.1088/0143-0807/26/5/023.

[25] R.H. Perry, D.W. Green, Section 12: psychrometry, evaporative cooling, and solids drying, in: Perry's Chemical Engineers' Handbook, seventh ed., The McGraw-Hill Companies, 1999, pp. 1154–1242.

[26] A. Sofo, A.S. Nimbran, Euler sums and integral connections, Mathematics 7 (9) (2019) 24.

[27] C.I. Ochoa-Martínez, H.S. Ramaswamy, A.A. Ayala-Aponte, Suitability of crank's solutions to Fick's second law for water diffusivity calculation and moisture loss prediction in osmotic dehydration of fruits, J. Food Process. Eng. 32 (2009) 933–943, https://doi.org/10.1111/j.1745-4530.2008.00254.x.

[28] E. Azuara, R. Cortés, H.S. Garcia, C.I. Beristain, Kinetic model for osmotic dehydration and its relationship with Fick's second law, Int. J. Food Sci. Technol. 27 (1992) 409–418.

[29] L.M. Cunha, F.A. Oliveira, J.C. Oliveira, Optimal experimental design for estimating the kinetic parameters of process described by the Weibull probability distribution function, J. Food Eng. 37 (1998) 175–191.

[30] L.M. Cunha, F.A. Oliveira, A.P. Aboim, J.M. Frıas, A. Pinheiro-Torres, Stochastic approach to the modelling of water losses during osmotic dehydration and improved parameter estimation, Int. J. Food Sci. Technol. 36 (2001) 253–262.

[31] B. Kaur, P. Rana, K. Sridhar, Mass transfer kinetics and process optimization of osmotic dehydration of Kinnow Mandarin (*Citrus reticulata*) peel, J. Food Process. Preserv. 46 (3) (2022), https://doi.org/10.1111/jfpp.16318.

[32] A.P. Zongo, S. Khalloufi, C. Ratti, Effect of viscosity and rheological behavior on selective mass transfer during osmotic dehydration of mango slices in natural syrups, J. Food Process. Eng. 44 (7) (2021), https://doi.org/10.1111/JFPE.13745.

[33] V. Ramya, N. Jain, A review on osmotic dehydration of fruits and vegetables: an integrated approach, J. Food Process. Eng. 40 (3) (2017), https://doi.org/10.1111/jfpe.12440.

[34] N.S. Md Salim, Y. Garièpy, V. Raghavan, Design of continuous flow osmotic dehydration and its performance on mass transfer exchange during osmotic dehydration of broccoli stalk slices, Food Bioprocess Technol. 9 (9) (2016) 1455–1470.

[35] Y. Feng, X. Yu, E.A. Yagoub, B. Xu, B. Wu, L. Zhang, C. Zhou, Vacuum pretreatment coupled to ultrasound assisted osmotic dehydration as a novel method for garlic slices dehydration, Ultrason. Sonochem. 50 (2019) 363–372.

[36] E.K. Dermesonlouoglou, F. Angelikaki, M.C. Giannakourou, G.J. Katsaros, P.S. Taoukis, Minimally processed fresh-cut peach and apricot snacks of extended shelf-life by combined osmotic and high-pressure processing, Food Bioprocess Technol. 12 (3) (2019) 371–386.

[37] K. Sethi, M. Kaur, Effect of osmotic dehydration on physicochemical properties of pineapple using honey, sucrose and honey-sucrose solutions, Int. J. Eng. Adv. Technol. 9 (1) (2019) 6257–6262.

[38] S.S. Sablani, M.S. Rahman, Effect of syrup concentration, temperature and sample geometry on equilibrium distribution coefficients during osmotic dehydration of mango, Food Res. Int. 36 (2003) 65–71.

[39] J.S. Alakali, C.C. Ariahu, N.N. Nkpa, Kinetics of osmotic dehydration of mango, J. Food Process. Preserv. 30 (2006) 597–607.

[40] A. Asghari, P.A. Zongo, E.F. Osse, S. Aghajanzadeh, V. Raghavan, S. Khalloufi, Review of osmotic dehydration: promising technologies for enhancing products' attributes, opportunities, and challenges for the food industries, Compr. Rev. Food Sci. Food Saf. 23 (2024) 13346.

[41] S. Erickson, J. Carr, The technological challenges of reducing the sugar content of foods, British Nutrition Foundation Nutrition Bulletin 45 (2020) 309–314, https://doi.org/10.1111/nbu.12454.